Vibrations Induced by Harmonic Loadings Applied at Circular Plate on Layered Medium

Gin-Show Liou

Journal of Mechanics / Volume 29 / Issue 02 / June 2013, pp 197 - 206
DOI: 10.1017/jmech.2012.137, Published online: 20 December 2012

VIBRATIONS INDUCED BY HARMONIC LOADINGS APPLIED AT CIRCULAR PLATE ON LAYERED MEDIUM

Gin-Show Liou *

Department of Civil Engineering
National Chiao-Tung University
Hsin-Chu, Taiwan 30049, R.O.C.

ABSTRACT

A systematic procedure is developed to calculate ground vibration at any specific location in layered medium due to harmonic loadings applied at a circular plate on the medium. In the procedure, the technique decomposing the interaction tractions between excited plate and layered medium will be employed. The decomposed tractions will automatically match boundary values of general solutions of three dimensional wave equations in cylindrical coordinates. In numerical results, the effect of layered stratum on ground vibration will be investigated and how ground vibration in layered medium decreases with depth will be presented. Also, from the numerical results, one can observe ground vibration may not decay monotonically along distance away from vibration source. The presented scheme is proved to be effective and efficient for accurately predicting near-field ground response to harmonic loadings applied at a rigid circular plate on layered medium. Comments on the presented scheme and numerical results will be given.

Keywords: Near-field, Ground vibrations, Layered medium, Wave propagation

1. INTRODUCTION

Ambient vibration due to near-by sources is annoying in design of vibration sensitive facility and hi-tech production machine. For vibration source, there are two major problems to be addressed in research; one is how to isolate or reduce vibration waves and the other is to evaluate attenuation of vibration waves. To deal with the first problem, open or in-fill trenches are usually recommended at the location near vibration source as Ahmad and Al-Hussaini [1] have suggested in their theoretical studies. Also, Lu *et al*. [2] have used pile row to reduce vibration caused by moving load. Moreover, if track is elevated on bridges, vibration due to excited bridge abutments also produce serious problem to hi-tech production machine and vibration sensitive facility. Takemiya [3] has designed a wave impeding barrier of honeycomb piles to reduce the vibrations near bridge abutments. As for evaluating wave attenuation due to different vibration sources, there are many researches. For examples, Sheng *et al*. [4] and Krylou [5] have employed Euler beam theory to model whole track including sleepers and ballast and then to solve the problem of moving train, and Kaynia *et al*. [6] have proposed a more sophisticated analysis model, which takes dynamic interaction into account, to evaluate ground vibration induced by passing trains. Moreover, Karlstrom [7] has employed a refined semi-analytic model to investigate the effect on ground vibration due to accelerating train.

Most of the above analysis model, finite element or boundary element methods are being used to model half-space medium or layered half-space medium. Regarding analytical approach to evaluate ground vibration, Yeh *et al*. have developed the transition matrix to calculate the ground vibration induced by incident and scattering wave [8]. Apsel and Ruco [9] have calculated the vibrations at the locations on half-space medium due to a point source (Green's Function). Vostroukhov [10] *et al*. have employed integral transform method to obtain ground vibration in layered half-space due to a buried uniform load at a circular area. And Liou [11,12] has developed a semi-analytical scheme to calculate vibration at arbitrary location on half-space medium and in half-space medium due to torsional, vertical, horizontal and rocking loads applied at a foundation plate on half-space surface. Also, from the practical point of view, Woods and Jedele [13] have collected some observed ground vibration data and deduced them into a simple formula expressing attenuation phenomenon of ground vibration in terms of soil damping and distance between source and observation locations. The paper will employ the technique, developed by Liou [11], to decompose the tractions induced by vibration of foundation plate. These decomposed tractions can match boundary values of general solutions of three dimensional wave equa-

* Corresponding author (gsliou@mail.nctu.edu.tw)

DOI : 10.1017/jmech.2012.137

tions in cylindrical coordinates. This technique has been applied to generating the impedance functions for circular foundation embedded in layered medium by Liou and Chung [14]. This paper will extend the work by Liou [11] to calculate the vibration at any location in layered medium induced by harmonic loadings applied at a rigid circular plate.

The analytical expression for vibration at a specific location in a layered medium will end up with a form of semi-infinite intergration with respect to wave number k, and Rayleigh singular pole existing in the integration path if there is no material damping effect in the medium. However, if material damping is always assigned in the medium, the singular pole will move away from intergration path. Therefore, from the decaying nature of the integrand with respect to k as shown in Liou's work [11], the vibration can be calculated by integration only up to a certain upper limit k_u without losing accuracy. Also, in the derivation, the interaction tractions between foundation plate and layered medium are assumed to be piecewise linear.

Some selected numerical results for a rigid circular plate subjected to torsional, vertical, horizontal and rocking excitations are presented to demonstrate the effectiveness and efficiency of the proposed scheme. In the numerical investigations, some numerical aspects regarding integration scheme, selection of k_u and influence of nondimensional layer thickness on the numerical scheme will be discussed. Also, some comments about the presented scheme are made.

2. ANALYTICAL SOLUTIONS FOR DYNAMIC LOADINGS ON LAYERED MEDIUM

The general solution of the differential equations for wave propagation in cylindrical coordinates is independently found for each layer in layered medium. The displacement and stress continuity conditions at the horizontal interfaces in layered system are then imposed in order to express the displacement and stress fields in terms of the prescribed dynamic loadings. The prescribed dynamic loadings are the interaction traction between foundation plate (vibration source) and surrounding medium. The total system of prescribed dynamic loadings applied at layered medium is shown in Fig. 1. The prescribed dynamic loadings can be expressed in cylindrical coordinates in terms of Fourier components with respect to azimuth as follows:

$$\begin{bmatrix} \overline{\tau_{rz}}(r,\ \theta) \\ \overline{\sigma_{zz}}(r,\ \theta) \\ \overline{\tau_{\theta z}}(r,\ \theta) \end{bmatrix} e^{i\omega t} = \sum_{n=0}^{1} \begin{bmatrix} \overline{\tau_{rz}}^{n}(r) \begin{Bmatrix} \cos(n\theta) \\ \sin(n\theta) \end{Bmatrix} \\ \overline{\sigma_{zz}}^{n}(r) \begin{Bmatrix} \cos(n\theta) \\ \sin(n\theta) \end{Bmatrix} \\ \overline{\tau_{\theta z}}^{n}(r) \begin{Bmatrix} -\sin(n\theta) \\ \cos(n\theta) \end{Bmatrix} \end{bmatrix} e^{i\omega t} \ ; \quad 0 \le r \le a_0 \ , \ z = 0 \tag{1}$$

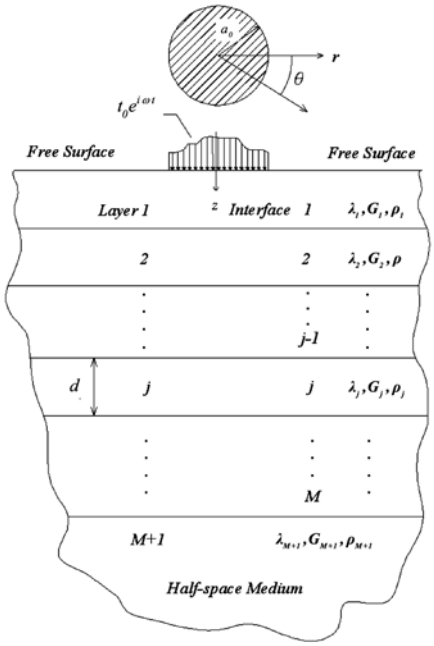

Fig. 1 Dynamic Loading on Layered Medium

where superscript n denotes nth Fourier component in the series; in this circular rigid plate case, $n = 0$ represents vertical (symmetric with respect to $\theta = 0$) and torsional (anti-symmetric with respect to $\theta = 0$) loadings, $n = 1$ represents horizontal and rocking (symmetric with respect to $\theta = 0$) loadings; ω is frequency; a_0 is radius of circular plate. Since the time variation $e^{i\omega t}$ appears on both sides of the equation, it will be omitted hereinafter.

Now, considering a particular layer j in the total system shown in Fig. 1, the general differential equations for wave propagation in the layer with harmonic excitation can be obtained using the technique separating the dilatational wave from the rotational wave. And the technique of separation of variables is employed to solve the independent differential equations for the dilatational wave and the rotational wave. After combining the solutions for the dilatational and the rotational waves, the general solution of the differential equations of wave propagation for nth Fourier component can be expressed in the matrix form as follows:

$$\begin{Bmatrix} u_r(r,\ z) & \begin{pmatrix} \cos n\theta \\ \sin n\theta \end{pmatrix} \\ u_z(r,\ z) & \begin{pmatrix} \cos n\theta \\ \sin n\theta \end{pmatrix} \\ u_\theta(r,\ z) & \begin{pmatrix} -\sin n\theta \\ \cos n\theta \end{pmatrix} \end{Bmatrix} = \begin{bmatrix} \begin{pmatrix} \cos n\theta \\ \sin n\theta \end{pmatrix} & 0 & 0 \\ 0 & \begin{pmatrix} \cos n\theta \\ \sin n\theta \end{pmatrix} & 0 \\ 0 & 0 & \begin{pmatrix} -\sin n\theta \\ \cos n\theta \end{pmatrix} \end{bmatrix} J\kappa_1 \, eA \tag{2}$$

or

$$\boldsymbol{Lu} = \boldsymbol{LJ}\boldsymbol{\kappa}_1\, \boldsymbol{eA}$$

where

$$J = \begin{bmatrix} J_n'(kr) & 0 & (n/r)\,J_n(kr) \\ 0 & kJ_n(kr) & 0 \\ (n/r)\,J_n(kr) & 0 & J_n'(kr) \end{bmatrix} \tag{3}$$

matrix $\boldsymbol{\kappa}_1$ is defined by Eq. (A-1) in Appendix, vector $\boldsymbol{A} = (A_1,\ B_1,\ C_1,\ A_2,\ B_2,\ C_2)^T$ is unknown coefficient vector determined from the boundary conditions at the upper and the lower interfaces of the layer, 6 × 6 diagonal matrix

$$e = diag(e^{-\nu_j z}\ , e^{-\nu_j' z}\ ,\ e^{-\nu_j' z}\ ,\ e^{\nu_j z}\ ,\ e^{\nu_j' z}\ ,\ e^{\nu_j' z})\ ,$$

$$\nu_j = \sqrt{k^2 - (\omega^2 / c_{pj}^2)}\ ,\ \nu_j' = \sqrt{k^2 - (\omega^2 / c_{gj}^2)}$$

c_{pj} and c_{gj} are compressional and shear wave velocities respectively in the layer (j^{th} layer), k is wave number in horizontal direction, $J_n(kr)$ is first kind of Bessel function of order n, and $J_n'(kr) = \left[dJ_n(kr)/dr\right]$.

The stress field in the layer can be obtained by differentiating the displacement field of Eq. (2) with respect to the corresponding variables r, z and θ, and then multiplying it with constitutive matrix of elasticity. The stress components on horizontal plane, with the azimuthal variation of matrix $\boldsymbol{L}$ in Eq. (2) factored out, can then be expressed as follows:

$$t = \begin{Bmatrix} \tau_{rz}(r,\ z) \\ \sigma_{zz}(r,\ z) \\ \tau_{\theta z}(r,\ z) \end{Bmatrix} = \boldsymbol{J}\boldsymbol{\kappa}_2\, \boldsymbol{eA} \tag{4}$$

where matrix $\boldsymbol{\kappa}_2$ is defined by Eq. (A-2) in Appendix.

Since the unknown coefficients in vector $\boldsymbol{A}$ are determined from the boundary conditions of the layer, the displacement and the stress fields of Eqs. (2) and (4) can be expressed in terms of the unknown displacement and stress components at the lower interface of the layer. Moreover, the displacement and stress components at the upper interface can be combined together and written in terms of the displacement and stress components at the lower interface as follows:

$$\boldsymbol{Y_{j-1}} = \boldsymbol{E}\boldsymbol{a}_j\, \boldsymbol{E^{-1}}\boldsymbol{Y_j} \tag{5}$$

where 6 × 6 matrix $\boldsymbol{E} = diag\ (\boldsymbol{J}, \boldsymbol{J})$ in which Bessel matrix $\boldsymbol{J}$ is shown in Eq.(3), transfer matrix $\boldsymbol{a}_j = \boldsymbol{\kappa e}^{-1}(d_j)\boldsymbol{\kappa}^{-1}$ in which matrix $\boldsymbol{\kappa} = [\boldsymbol{\kappa}_1^T,\ \boldsymbol{\kappa}_2^T]^T$ is defined by Eq. (A-3) in Appendix , diagonal matrix $\boldsymbol{e}(d_j) = \boldsymbol{e}\,|_{z=d_j}$ in which d_j is the thickness of the layer, and $\boldsymbol{Y}_{j-1}$ and $\boldsymbol{Y}_j$ are the unknown displacement-stress vectors at the upper and the lower interfaces of the layer, respectively.

Consider the total system shown in Fig. 1. For a given layer in the system, Eq. (5) shows that the displacement-stress vector at the upper interface can be expressed in terms of the displacement –stress vector at the lower interface. Therefore, by imposing the displacement and stress continuity conditions at the horizontal interfaces from the first top layer down to the half-space layer, one can obtain the displacement-stress vector at the surface of the total system in terms of the displacement-stress vector at the surface of the half-space layer as expressed by Eq. (6).

$$\boldsymbol{Y_0} = \boldsymbol{E}\boldsymbol{a_1}\boldsymbol{a_2}.....\boldsymbol{a_M}\,\boldsymbol{E^{-1}}\boldsymbol{Y_M} = \boldsymbol{ETE^{-1}}\boldsymbol{Y_M} \tag{6}$$

Consider the half-space layer in Fig. 1 alone. The general solutions of differential equations of wave propagation and the stress field in the half-space layer are similar to Eqs. (2) and (4) respectively except that upward propagating reflection waves do not exist. The displacement-stress vector at the surface of the half-space layer can then be written as

$$\boldsymbol{Y_M} = \begin{Bmatrix} \boldsymbol{u_M} \\ \boldsymbol{t_M} \end{Bmatrix} = \boldsymbol{E}\boldsymbol{\kappa}'\boldsymbol{A}' \tag{7}$$

where matrix $\boldsymbol{\kappa}' = [\boldsymbol{\kappa}_1'^T\ ,\ \boldsymbol{\kappa}_2'^T]^T$ in which submatrices $\boldsymbol{\kappa}_1'$ and $\boldsymbol{\kappa}_2'$ are defined by Eqs. (A-1a) and (A-2a) in Appendix respectively, and $\boldsymbol{A}' = (A_1,\ B_1,\ C_1)^T$ is unknown coefficient vector determined from the boundary conditions at the surface of the half-space layer.

Substituting $\boldsymbol{Y_M}$ in Eq. (7) into Eq. (6) , Eq. (6) can be written as

$$\boldsymbol{Y_0} = \begin{Bmatrix} \boldsymbol{u_0} \\ \boldsymbol{t_0} \end{Bmatrix} = \begin{bmatrix} \boldsymbol{J} & \boldsymbol{0} \\ \boldsymbol{0} & \boldsymbol{J} \end{bmatrix} \begin{bmatrix} \boldsymbol{T_{11}} & \boldsymbol{T_{12}} \\ \boldsymbol{T_{21}} & \boldsymbol{T_{22}} \end{bmatrix} \begin{bmatrix} \boldsymbol{\kappa}_1' \\ \boldsymbol{\kappa}_2' \end{bmatrix} \boldsymbol{A}' \tag{8}$$

where $T_{11} \sim T_{22}$ are submatrices of matrix T in Eq. (6). After some matrix manipulations of eliminating the unknown vector $\boldsymbol{A}'$, one can obtain the displacement vector $\boldsymbol{u_0}$ in terms of the stress vector $\boldsymbol{t_0}$.

$$\boldsymbol{u_0} = \boldsymbol{J}(\boldsymbol{T_{11}}\,\boldsymbol{\kappa}_1' + \boldsymbol{T_{12}}\,\boldsymbol{\kappa}_2')(\boldsymbol{T_{21}}\,\boldsymbol{\kappa}_1' + \boldsymbol{T_{22}}\,\boldsymbol{\kappa}_2')^{-1}\boldsymbol{J^{-1}}\boldsymbol{t_0} = \boldsymbol{JQJ^{-1}}\boldsymbol{t_0} \tag{9}$$

If the layered medium is assumed to be welded to a rigid lower boundary, then $\boldsymbol{u_M} = \boldsymbol{0}$ in $\boldsymbol{Y_M}$ of Eq. (6). This leads to $\boldsymbol{Q} = \boldsymbol{T_{12}}\boldsymbol{T_{22}^{-1}}$ for Eq. (9).

Equation (9) shows the relationship of the stress and the displacement vectors on the surface of the total system. This means that one can calculate vibration at arbitrary location on the surface due to the vibration source of Eq. (1), if Eq. (1) is properly decomposed to match $\boldsymbol{t_0}$ in Eq.(9). The method to decompose Eq. (1) has been proposed by Liou [11], and will be summarized later.

To calculate vibration at locations in an arbitrary layer j shown in Fig. 1, one has to calculate the displacement-stress vector $\boldsymbol{Y}_{j-1}$ at interface $j-1$ first. From Eq.(6), one observes that $\boldsymbol{Y}_{j-1}$ can be expressed in terms of $\boldsymbol{Y_0}$ as follows:

$$\boldsymbol{Y_{j-1}} = \boldsymbol{E}\boldsymbol{a}_{j-1}^{-1}.....\boldsymbol{a}_1^{-1}\boldsymbol{E^{-1}}\boldsymbol{Y_0} = \boldsymbol{ET'E^{-1}}\boldsymbol{Y_0} \tag{10}$$

where matrices $\boldsymbol{E}$ and a_1……a_{j-1} are respectively defined in Eq. (5) and Eq. (A-3) in Appendix.

Now considering the solution for layer j alone, the general solutions for displacement and stress on horizontal plane in layer j are given by Eqs. (2) and (4), respectively. One can assemble the two equations as follows:

$$\boldsymbol{Y} = \begin{Bmatrix} \boldsymbol{u} \\ \boldsymbol{t} \end{Bmatrix} = \boldsymbol{E} \begin{Bmatrix} \boldsymbol{\kappa}_1 \\ \boldsymbol{\kappa}_2 \end{Bmatrix} \boldsymbol{eA} \tag{11}$$

where matrices $\boldsymbol{E}$, $\boldsymbol{\kappa}_1$, $\boldsymbol{\kappa}_2$, $\boldsymbol{e}$ and vector $\boldsymbol{A}$ of unknown coefficients are respectively defined in Eqs. (2), (4) and (5). Equation (11) can be employed to calculate the displacement and stress components at interface $j-1$ by setting $z = 0$. Equation (11) becomes

$$\boldsymbol{Y}_{j-1} = \boldsymbol{E} \begin{Bmatrix} \boldsymbol{\kappa}_1 \\ \boldsymbol{\kappa}_2 \end{Bmatrix} \boldsymbol{A} \tag{12}$$

This leads to

$$\boldsymbol{A} = \begin{Bmatrix} \boldsymbol{\kappa}_1 \\ \boldsymbol{\kappa}_2 \end{Bmatrix}^{-1} \boldsymbol{E}^{-1} \boldsymbol{Y}_{j-1} \tag{13}$$

Substituting Eq. (13) into Eq.(11), one obtains

$$\boldsymbol{Y} = \boldsymbol{E} \begin{Bmatrix} \boldsymbol{\kappa}_1 \\ \boldsymbol{\kappa}_2 \end{Bmatrix} \boldsymbol{e} \begin{Bmatrix} \boldsymbol{\kappa}_1 \\ \boldsymbol{\kappa}_2 \end{Bmatrix}^{-1} \boldsymbol{E}^{-1} \boldsymbol{Y}_{j-1} = \boldsymbol{E} \boldsymbol{a}_j' \boldsymbol{E}^{-1} \boldsymbol{Y}_{j-1} \tag{14}$$

where matrix $\boldsymbol{a}_j'$ can be expressed in a similar form of $\boldsymbol{a}_j$ with d_j replaced with z in Eq. (A-3). Now, substituting Eq. (10) into Eq. (14) , the displacement and stress components on arbitrary horizontal plane at depth z from the interface $j-1$ can be obtained as follows:

$$\boldsymbol{Y} = \boldsymbol{E} \boldsymbol{a}_j' \boldsymbol{T}' \boldsymbol{E}^{-1} \boldsymbol{Y}_0 = \boldsymbol{E} \boldsymbol{Q}' \boldsymbol{E}^{-1} \boldsymbol{Y}_0 \tag{15}$$

Using Eq. (9) to assemble vector $\boldsymbol{Y}_0$ $(\boldsymbol{Y}_0 = (\boldsymbol{u}_0^T, \boldsymbol{t}_0^T)^T)$, vector $\boldsymbol{Y}$ can be expressed as

$$\boldsymbol{Y} = \begin{Bmatrix} \boldsymbol{u} \\ \boldsymbol{t} \end{Bmatrix} = \boldsymbol{E} \boldsymbol{Q}' \begin{Bmatrix} \boldsymbol{Q} \\ \boldsymbol{I} \end{Bmatrix} \boldsymbol{J}^{-1} \boldsymbol{t}_0 \tag{16}$$

where matrices $\boldsymbol{E}$, $\boldsymbol{Q}'$, $\boldsymbol{Q}$ and $\boldsymbol{J}$ are defined in Eqs. (5), (15), (9) and (3) respectively, and matrix $\boldsymbol{I}$ is 3×3 identity matrix. Therefore, the displacement vector $\boldsymbol{u}$ in Eq. (16) can be obtained as follows :

$$\boldsymbol{u} = \boldsymbol{J}(\boldsymbol{Q}_{11}' \boldsymbol{Q} + \boldsymbol{Q}_{12}') \boldsymbol{J}^{-1} \boldsymbol{t}_0 \tag{17}$$

where 3×3 matrices $\boldsymbol{Q}_{11}'$ and $\boldsymbol{Q}_{12}'$ are submatrices of 6×6 matrix $\boldsymbol{Q}'$ in Eq. (15) as $\boldsymbol{Q}'$ can be partitioned as follows:

$$\boldsymbol{Q}' = \begin{bmatrix} \boldsymbol{Q}_{11}' & \boldsymbol{Q}_{12}' \\ \boldsymbol{Q}_{21}' & \boldsymbol{Q}_{22}' \end{bmatrix} \tag{17a}$$

To calculate vibrations in half-space layer in Fig.1, one can express the unknown coefficient vector $\boldsymbol{A}'$ in Eq. (7) by using Eq. (8) as follows :

$$\boldsymbol{A}' = (\boldsymbol{T}_{21} \boldsymbol{\kappa}_1' + \boldsymbol{T}_{22} \boldsymbol{\kappa}_2')^{-1} \boldsymbol{J}^{-1} \boldsymbol{t}_0 \tag{17b}$$

Similar to Eq. (17), the displacement vector at arbitrary location (depth z) in half-space layer can then be expressed as follows :

$$\boldsymbol{u} = \boldsymbol{J} \boldsymbol{\kappa}_1' \boldsymbol{e}' \boldsymbol{A}' = \boldsymbol{J} \boldsymbol{\kappa}_1' \boldsymbol{e}' (\boldsymbol{T}_{21} \boldsymbol{\kappa}_1' + \boldsymbol{T}_{22} \boldsymbol{\kappa}_2')^{-1} \boldsymbol{J}^{-1} \boldsymbol{t}_0 \tag{17c}$$

where 3×3 diagonal matrix $\boldsymbol{e}' = diag(e^{-\nu_{M+1} z}, e^{-\nu_{M+1}' z}, e^{-\nu_{M+1}' z})$ is similar to the 6×6 diagonal matrix e defined in Eq. (2).

Equations (17) and (17c) give the displacement vector $\boldsymbol{u}$ at arbitrary location in arbitrary layer j and in half-space layer $M+1$, respectively, of the total system in Fig. 1, if traction vector $\boldsymbol{t}_0$ applied at the surface of the total system is known.

To obtain traction vector $\boldsymbol{t}_0$, Liou [11] has developed a technique to decompose the interaction tractions of Eq. (1) by approximating each Fourier component of interaction tractions with piecewise linear distribution in r-direction first as follows:

$$\begin{aligned} \overline{\tau_{rz}}^{n} &= \sum_{j=1}^{m-1} h_j(r) p_j + h_0(r) p_0 + h_m(r) p_m = \boldsymbol{h}^T \boldsymbol{p} \\ \overline{\sigma_{zz}}^{n} &= \sum_{j=1}^{m-1} h_j(r) q_j + h_0(r) q_0 + h_m(r) q_m = \boldsymbol{h}^T \boldsymbol{q} \\ \overline{\tau_{\theta z}}^{n} &= \sum_{j=1}^{m-1} h_j(r) s_j + h_0(r) s_0 + h_m(r) s_m = \boldsymbol{h}^T \boldsymbol{s} \end{aligned} \tag{18}$$

where

$$h_j(r) = \begin{cases} 1 + \dfrac{r - jb}{b}, & \text{if } (j-1)b \le r \le jb \text{ and } 1 \le j \le m \\ 1 - \dfrac{r - jb}{b}, & \text{if } jb \le r \le (j+1)b \text{ and } 0 \le j \le m-1 \\ 0, & otherwise \end{cases} \tag{18a}$$

$b = a_0 / m$ is width of subinterval, m is number of subintervals, and p_j, q_j and s_j are the traction intensities at node j for $\overline{\tau_{rz}}^{n}$, $\overline{\sigma_{zz}}^{n}$ and $\overline{\tau_{\theta z}}^{n}$ respectively.

After some mathematical manipulation as shown in Liou's work [11], one can obtain the following equation.

$$\overline{\boldsymbol{t}_0} = \begin{bmatrix} \overline{\tau_{rz}}^{n} \\ \overline{\sigma_{zz}}^{n} \\ \overline{\tau_{\theta z}}^{n} \end{bmatrix} = \int_0^{\infty} \boldsymbol{J} \begin{bmatrix} -\boldsymbol{D}_{n+1}^T + \boldsymbol{D}_{n-1}^T & \boldsymbol{0} & \boldsymbol{D}_{n+1}^T + \boldsymbol{D}_{n-1}^T \\ \boldsymbol{0} & \boldsymbol{D}_n^T & \boldsymbol{0} \\ \boldsymbol{D}_{n+1}^T + \boldsymbol{D}_{n-1}^T & \boldsymbol{0} & -\boldsymbol{D}_{n+1}^T + \boldsymbol{D}_{n-1}^T \end{bmatrix} \begin{Bmatrix} \boldsymbol{p} \\ \boldsymbol{q} \\ \boldsymbol{s} \end{Bmatrix} dk = \int_0^{\infty} \boldsymbol{JDP} dk \tag{19}$$

where

$$\begin{aligned} \boldsymbol{D}_{n+1}^T &= \int_0^{a_0} \frac{r}{2} J_{n+1}(kr) \, \boldsymbol{h}^T dr \\ \boldsymbol{D}_n^T &= \int_0^{a_0} r J_n(kr) \, \boldsymbol{h}^T dr \end{aligned} \tag{19a}$$

and

$$\boldsymbol{D}_{n-1}^{T} = \int_0^{a_0} \frac{r}{2} J_{n-1}(kr)\, \boldsymbol{h}^{T} dr$$

Equation (19a) is Hankel transform of Eq. (18). Thereforce, ground surface is no longer traction free for each wave number k. Using $\boldsymbol{t}_0 = -\overline{\boldsymbol{t}_0}$ and substituting $\boldsymbol{t}_0 = -\boldsymbol{JDP}dk$ from Eq. (19) into Eq. (17) or Eq. (17c), the displacement vector at arbitrary depth in arbitrary layer or in half-space layer, respectively, can be obtained by integrating the resulting expression from 0 to ∞.

$$\boldsymbol{u} = -\int_0^{\infty} \boldsymbol{J}(\boldsymbol{Q}_{11}'\boldsymbol{Q} + \boldsymbol{Q}_{12}')\, \boldsymbol{DP}dk \tag{20}$$

or

$$\boldsymbol{u} = -\int_0^{\infty} \boldsymbol{J}\boldsymbol{\kappa}_1' \boldsymbol{e}'(\boldsymbol{T}_{21}\boldsymbol{\kappa}_1' + \boldsymbol{T}_{22}\boldsymbol{\kappa}_2')^{-1}\, \boldsymbol{DP}dk \tag{20a}$$

Equations (20) or (20a) can be employed to calculate vibration at any specific location in layered medium, if the intensity vector $\boldsymbol{P} = [\boldsymbol{p}^T, \boldsymbol{q}^T, \boldsymbol{s}^T]^T$ described in Eq. (18) is known.

Also, one should note that intensity vector $\boldsymbol{P}$ is independent of wave number k.

To find the intensity vector $\boldsymbol{P}$ due to harmonic loading applied at foundation plate, the impedance matrix (dynamic stiffness matrix) for the plate has to be obtained first. The methodology of finding impedance matrix has been presented by Liou [14]. In the methodology, finite element model for displacement field of foundation is assumed, and variational principle (principle of virtual work) and reciprocal theorem are employed. Then, the intensity vector $\boldsymbol{P}$ in Eqs. (18) or (19) can be obtained for all the excitation forces and moments in the process of finding impedance matrix.

For the cases of rigid circular foundation, the displacement fields in the foundation plate can be assumed as follows:

$u_\theta(r, \theta) = \upsilon_1 r$ (n = 0 of anti-symmetric mode) for excitation by torsional moment, $u_z(r, \theta) = \upsilon_2$ (n = 0 of symmetric mode) for excitation by vertical force, and $u_z(r, \theta) = \upsilon_3 r\cos\theta$, $u_r(r, \theta) = \upsilon_4 \cos\theta$ and $u_\theta(r, \theta) = -\upsilon_4 \sin\theta$ (n = 1 of symmetric mode) for excitations by rocking moment and horizontal force.

In the expressions, υ_1 is the unknown generalized displacement at center of foundation for torsional excitation, υ_2 is for vertical excitation, and υ_3 and υ_4 are, respectively, for coupling rocking and horizontal excitations.

With these assumed displacement fields of foundation plate, the impedance matrix and the interaction tractions in Eq. (18) can therefore be calculated for a rigid circular foundation subjected to harmonic loadings. Then, the displacement vector $\boldsymbol{u}$ in Eqs. (20) or (20a) can be calculated.

3. NUMERICAL INVESTIGATIONS

The semi-infinite integration of Eqs. (20) or (20a) can be replaced with finite integration without losing accuracy, if material damping is always assumed in the medium and nondimensional integration limit (normalized by shear wave length λ of top layer) k_u, to replace ∞ for Eqs. (20) or (20a), is properly chosen. This has been proved by Liou [11] using decaying nature with respect to wave number k for the elements in matrices J, Q and D in Eqs. (20) or (20a). Also, Liou [11] has verified the presented scheme by comparison of the results with that by point source (Green Function) applied on half-space medium. Two-layer system (one layer over half-space) is used to perform the numerical investigation. The investigation concludes that nondimensional integration limit k_u can be smaller as nondimensional thickness (normalized by shear wave length λ of top layer) d_1 is greater, and nondimensional integration limit k_u must be larger as shear modulus ratio (G_2 / G_1) is greater or nondimensional distance r (normalized by shear wave length of top layer) from center of vibration source is farther. For examples: Nondimensional integration limit k_u = 5,000 is large enough for the case of (G_2 / G_1) = 5 and nondimensional top layer thickness d_1 = 1 with ground vibrations to be calculated for locations of nondimensional distance r up to 10; nondimensional integration limit k_u must be as large as 50,000 for the case of (G_2 / G_1) = 100 and nondimensional top layer thickness d_1 = 0.1 with ground vibrations to be calculated for locations of non-dimensional distance r only up to 2. Also, by comparing the cases of torsional, vertical, horizontal and rocking excitations to each other, larger k_u is necessary for the case of torsional excitation if one wants to obtain the same accurate results. Figure 2 shows the converging results by different k_u (10000, 20000, 30000, 40000, 50000 and 60000) for the case of excitation by unit nondimensional torsional moment. From the figure, one can see that the amplitude of nondimensional displacement $|u_\theta|$ (normalized by shear wave length) at z = 0 has been converging as k_u = 50,000 for nondimensional distances r = 0 ~ 2. To calculate the results in Fig. 2, following parameters are selected: Nondimensional top layer thickness d_1 = 0.1; nondimensional frequency ω = 1.0 (normalized by thickness and shear wave velocity of top layer; *i.e.* $\lambda d_1 \overline{\omega} / 2\pi c_{s1}$); nondimensional plate radius a_0 = 0.01 (normalized by shear wave length of top layer); Poisson ratio is 0.33; damping ratio of layered medium is 0.05; shear modulus ratio (G_2 / G_1) = 100.

Since the torsional, vertical, horizontal, coupling and rocking impedances for circular plate are nondimensionalized, respectively, as $I_{TT} / G_1 a_0^3$, $I_{\upsilon\upsilon} / G_1 a_0$, $I_{HH} / G_1 a_0$, $I_{HR} / G_1 a_0$ and $I_{RR} / G_1 a_0^3$ as defined in

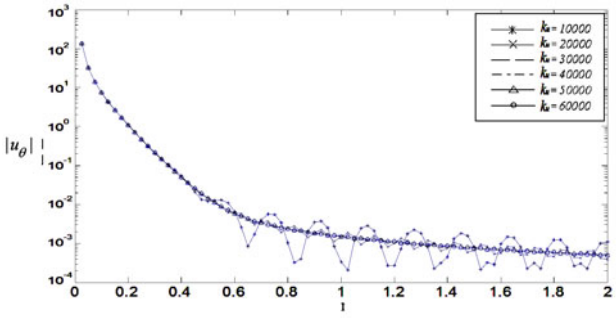

Fig. 2 Converging Results for soft layer over stiff half-space medium subjected to torsional excitation ($Z = 0$)

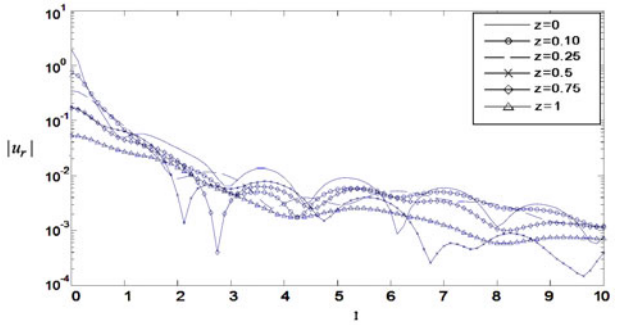

Fig. 3 Vibration amplitude of u_r due to unit nondimensional horizontal force ($a_0 = 0.1$)

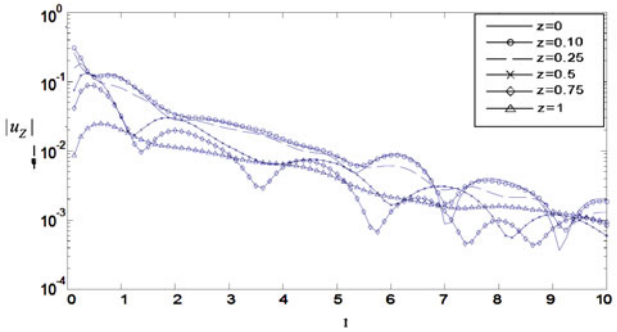

Fig. 4 Vibration amplitude of u_z due to unit nondimensional horizontal force ($a_0 = 0.1$)

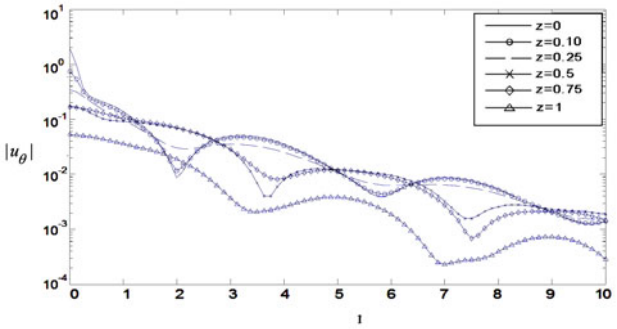

Fig. 5 Vibration amplitude of u_θ due to unit nondimensional horizontal force ($a_0 = 0.1$)

Liou and Chung's work [14], the excitation forces are normalized in the similar way. The vertical and horizontal excitation forces are nondimensionalized in the forms of $F_V / G_1 a_0 \lambda$ and $F_H / G_1 a_0 \lambda$, respectively, in which λ is the shear wave length of top layer. The torsional and rocking excitation moments are normalized in the forms of $M_T / G_1 a_0^3 \lambda$ and $M_R / G_1 a_0^3 \lambda$, respectively. Because these quantities have been manipulated in this way, the numerical results of u_r, u_z and u_θ will also be nondimensionalized by λ. The numerical results discussed in the paper are calculated with unit nondimensionalized harmonic excitation forces applied at foundation. This means the excitation forces $F_v = G_1 a_0 \lambda$, $F_H = G_1 a_0 \lambda$, $M_T = G_1 a_0^3 \lambda$ and $M_R = G_1 a_0^3 \lambda$.

The effect of the number of subinterval m for piecewise linear model in Eq. (18) on the numerical precision is also investigated. Table 1 shows some results of u_r and u_z at groud surface ($z = 0$) due to unit nondimesional vertical force.

The parameters chosen to calculate the results of Table 1 and Figs. 3, 4 and 5 are as follows: Nondimensional plate radius $a_0 = 0.1$; nondimensional frequency $\omega = 1.0$; nondimensional thickness of top layer $d_1 = 1.0$; Poisson ratio is 0.33; damp ratio is 0.05 for both layers (bottom half-space layer and top layer); shear modulus ratio of bottom half-space layer to top layer $G_2 / G_1 = 5.0$.

From Table 1, one can observe that the effect of number of subinterval m on results is diminishing as the nondimensional distance r goes farther. For example, the difference between the results for $m = 1$ and $m = 20$ is less than 1% for $r = 1.0$. This means the variation of distribution of interaction tractions is not an important factor for ground vibrations as nondimensional distance getting larger.

Gaussian quadrature is employed to perform the integrations of matrix $\boldsymbol{D}$ in Eq. (19) and displacement vector $\boldsymbol{u}$ in Eqs. (20) or (20a), and the number of subintervals $m = 20$ in Eq. (18) is selected for the numerical results presented in the paper. All the integration schemes employed in presented procedure have been carefully checked in order to ensure that the number of the significant figures of the final numerical results (u_r, u_z and u_θ) is no less than 4. Also, depth z for calculating the displacement amplitudes shown in Figs. 3 ~ 10 is normalized by shear wave length λ of top layer. Figs. 3, 4 and 5 show the nondimensional amplitude $|u_r|$, $|u_z|$ and $|u_\theta|$ respectively for the case of foundation plate subjected to unit nondimensional horizontal force. From these figures, one can observe that ground vibration, in average, decreases with depth, although fluctuation along nondimensional distance occurs. The fluctuation seems no fixed pattern. This indicates that near-field vibration due to wave propagation in layered medium is more unpredictable than far-field vibration. From Figs. 3, 4 and 5, it can be confirmed that foundation of structure can be embedded in ground in order to reduce the influence of ground vibration.

The results for u_r, u_z and u_θ shown in Figs. 6, 7 and 8 respectively are for the case of $a_0 = 0.1$ in contrast to that in Figs. 3 ~ 5. From these 3 figures, one can

Table 1 Ground Vibrations due to unit nondimensional vertical force ($a_0 = 0.1$)

r \ u		u_r		u_z	
	m	Re	Im	Re	Im
0	$m = 1$	0.000000E+00	0.000000E+00	1.170450E+00	−7.719510E-01
	$m = 10$	0.000000E+00	0.000000E+00	1.268820E+00	−7.737340E-01
	$m = 20$	0.000000E+00	0.000000E+00	1.264420E+00	−7.727760E-01
0.125	1	−1.482910E-01	9.119650E-02	5.431670E-01	−6.606440E-01
	10	−1.438410E-01	8.708790E-02	5.575520E-01	−6.598690E-01
	20	−1.433740E-01	8.670190E-02	5.587060E-01	−6.597910E-01
0.25	1	−2.717150E-02	1.397540E-01	−1.114250E-01	−3.428860E-01
	10	−2.711180E-02	1.383050E-01	−1.091560E-01	−3.421740E-01
	20	−2.708120E-02	1.381670E-01	−1.089700E-01	−3.421170E-01
0.375	1	7.909590E-02	9.050190E-02	−2.235130E-01	−6.169320E-02
	10	7.846670E-02	8.974590E-02	−2.221000E-01	−6.220600E-02
	20	7.842310E-02	8.967050E-02	−2.219810E-01	−6.225570E-02
0.5	1	1.185460E-01	−5.926990E-03	−1.391100E-01	1.116700E-01
	10	1.177740E-01	−5.993480E-03	−1.386760E-01	1.106490E-01
	20	1.177110E-01	−6.006480E-03	−1.386430E-01	1.105570E-01
0.625	1	8.333560E-02	−9.362590E-02	−3.639840E-04	1.453970E-01
	10	8.284420E-02	−9.319620E-02	−7.580230E-04	1.446060E-01
	20	8.280280E-02	−9.316420E-02	−7.974330E-04	1.445370E-01
0.75	1	2.980070E-03	−1.284150E-01	9.182190E-02	7.547550E-02
	10	2.952060E-03	−1.278490E-01	9.110030E-02	7.531040E-02
	20	2.949120E-03	−1.278040E-01	9.103360E-02	7.529830E-02
0.875	1	−7.417010E-02	−9.920670E-02	9.620140E-02	−2.270950E-02
	10	−7.382990E-02	−9.884610E-02	9.569030E-02	−2.231170E-01
	20	−7.380160E-02	−9.881770E-02	9.564380E-02	−2.227330E-02
1	1	−1.085530E-01	−2.965630E-02	3.334090E-02	−8.033340E-01
	10	−1.081160E-01	−2.965540E-02	3.332250E-02	−7.974970E-02
	20	−1.080800E-01	−2.965730E-02	3.332160E-02	−7.969530E-02

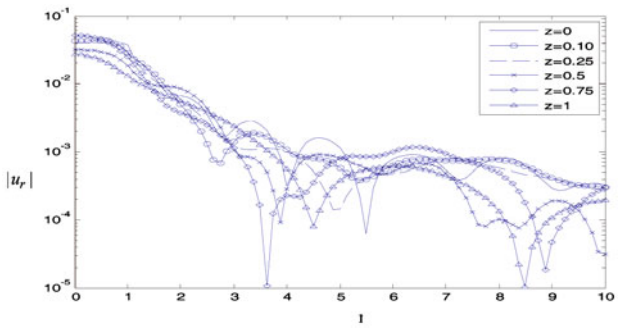

Fig. 6 Vibration amplitude of u_r due to unit nondimensional horizontal force ($a_0 = 0.1$)

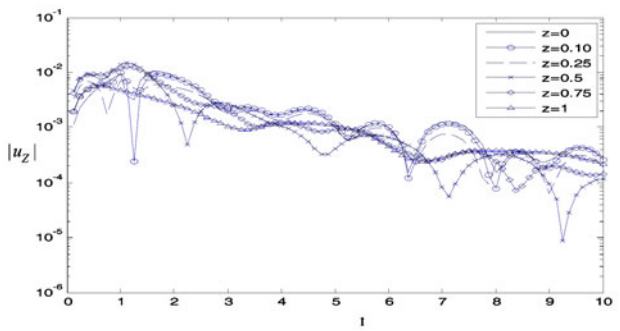

Fig. 7 Vibration amplitude of u_z due to unit nondimensional horizontal force ($a_0 = 0.1$)

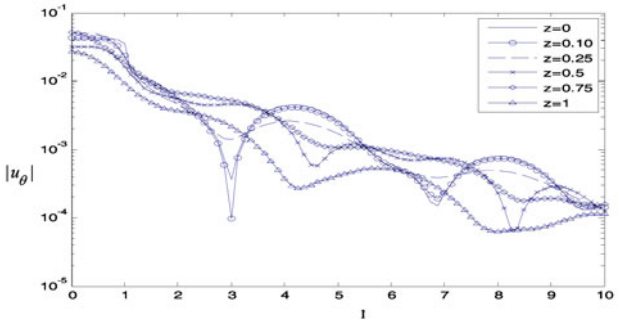

Fig. 8 Vibration amplitude of u_θ due to unit nondimensional horizontal force ($a_0 = 0.1$)

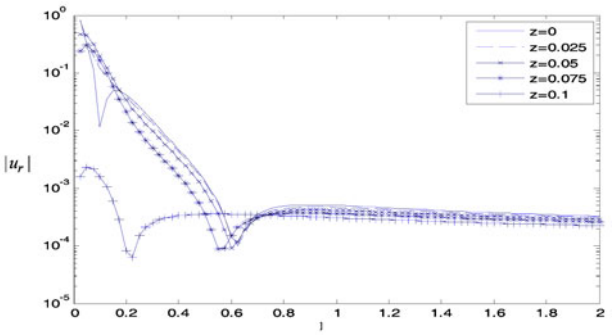

Fig. 9 Vibration amplitude of u_r due to unit nondimensional vertical force for thin layer situation

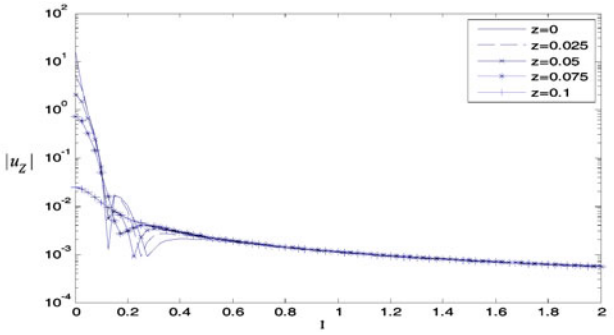

Fig. 10 Vibration amplitude of u_z due to unit nondimensional vertical force for thin layer situation

observe that the ground vibration may not decay with depth in average as the ground location (r) is very close to vibration source (circular plate). This phenomenon is not observed in Figs. 3, 4 and 5 for the case of $a_0 = 0.1$.

The behavior of harmonic wave propagation in a thin soft layer over stiff half-space layer is also investigated in the paper. In the investigation, except $d_1 = 0.1$, $a_0 = 0.01$, $k_u = 50000$ and $G_2 / G_1 = 100$ are assigned, the other parameters are the same as the parameter chosen for the case to calculate the results in Figs. 3 ~ 8. The results of nondimensional displacement amplitude $| u_r |$ and $| u_z |$ for the case of vertical excitation by unit nondimensional force are shown in Figs. 9 and 10. In the two figures, one can observe two characteristics as follows: (1) The decay of vibration along horizontal nondimensional distance is very fast for $r < 0.8$; (2) For $r > 0.8$, the vibration decays monotonically. From characteristics No. (2), one can conclude that thin layer provides as wave guide for nondimensional distance $r > 0.8$. This also indicates that the fluctuation phenomenon shown in Figs. 3 ~ 8 is diminishing as the ratio r/d_1 is getting larger and larger. To obtain the results with $r > 2$, one can extrapolate the results shown in Figs. 9 and 10 linearly in log-scale. Although only the results for vertical excitation are shown in Figs. 9 and 10, the results for torsional, horizontal and rocking excitations also indicate the same characteristics stated above.

4. CONCLUSIONS

The presented method is very effective and efficient for calculating the near-field ground vibration in layered medium, since the numerical scheme is convergent. This convergency can be proved by comparison of the numerical results calculated with increasing number of integration points or shortening the integration interval while using Gaussian Quadrature to integrate Eqs. (19a), (20) and (20a), or like the results shown in Fig. 2 by selecting larger integration upper limit k_u to replace ∞ in Eqs. (20) or (20a). From Figs. 3, 4 and 5, one can observe that ground vibration, in average, is smaller as depth is getting greater. This means that deeper foundation for building to house vibration sensitive facility is effective. However, this statement may not valid as the vibration source is very close to the facility. This can be observed in Figs. 6, 7 and 8. Moreover, from Figs. 9 and 10, one can conclude that layer can act like a wave guide, if the thickness of the layer compared to wave length is small. Also, from Figs. 9, 10 and other numerical results not shown in the paper, one can conclude that the fluctuation phenomenon is diminishing as the ratio r/d_1 (nondimensional distance to nondimensional thickness of top layer) is getting larger.

ACKNOWLEDGMENTS

The financial support of this research is partly provided by National Science Council of Taiwan through Contract no. 98-2221-E-009-098.

APPENDIX

The matrix $\boldsymbol{\kappa}_1$ in Eq. (2) can be expressed as follows:

$$\boldsymbol{\kappa}_1 = [\boldsymbol{\kappa}_1' \quad \boldsymbol{\kappa}_1''] \tag{A-1}$$

where

$$\boldsymbol{\kappa}_1' = \begin{bmatrix} k & -\nu_j' & 0 \\ -\nu_j & k & 0 \\ 0 & 0 & 1 \end{bmatrix} \tag{A-1a}$$

and

$$\boldsymbol{\kappa}_1'' = \begin{bmatrix} k & v_j' & 0 \\ v_j & k & 0 \\ 0 & 0 & 1 \end{bmatrix} \tag{A-1b}$$

The matrix $\boldsymbol{\kappa}_2$ in Eq. (4) can be expressed as follows:

$$\boldsymbol{\kappa}_2 = [\boldsymbol{\kappa}_2' \quad \boldsymbol{\kappa}_2''] \tag{A-2}$$

where

$$\boldsymbol{\kappa}_2' = \begin{bmatrix} -2kG_j v_j & G_j(2k^2 - k_{\beta_j}^2) & 0 \\ G_j(2k^2 - k_{\beta_j}^2) & -2kG_j v_j' & 0 \\ 0 & 0 & -G_j v_j' \end{bmatrix} \tag{A-2a}$$

and

$$\boldsymbol{\kappa}_2'' = \begin{bmatrix} 2kG_j v_j & G_j(2k^2 - k_{\beta_j}^2) & 0 \\ G_j(2k^2 - k_{\beta_j}^2) & 2kG_j v_j' & 0 \\ 0 & 0 & G_j v_j' \end{bmatrix} \tag{A-2b}$$

in which $k_{\beta_j}^2 = \omega^2 / c_{gj}^2$, G_j is shear modulus of jth layer.

The transfer matrix $\boldsymbol{a_j}$ in Eq. (5) can be expressed as follows:

$$\boldsymbol{a_j} = \begin{bmatrix} \boldsymbol{a_{11}} & \boldsymbol{a_{12}} \\ \boldsymbol{a_{21}} & \boldsymbol{a_{22}} \end{bmatrix} \tag{A-3}$$

where

$$\boldsymbol{a_{11}} = \begin{bmatrix} \frac{2k^2}{k_{\beta_j}^2}(CH - CH') + CH' & \frac{k}{k_{\beta_j}^2}\left((2k^2 - k_{\beta_j}^2)\frac{SH}{v_j} - 2v_j' SH'\right) & 0 \\ \frac{k}{k_{\beta_j}^2}\left(-2v_j\, SH + (2k^2 - k_{\beta_j}^2)\frac{SH'}{v_j'}\right) & CH - \frac{2k^2}{k_{\beta_j}^2}(CH - CH') & 0 \\ 0 & 0 & CH' \end{bmatrix} \tag{A-3a}$$

$$\boldsymbol{a_{12}} = \begin{bmatrix} \frac{1}{G_j k_{\beta_j}^2}\left(v_j' SH' - k^2 \frac{SH}{v_j}\right) & \frac{-k}{G_j k_{\beta_j}^2}(CH - CH') & 0 \\ \frac{k}{G_j k_{\beta_j}^2}(CH - CH') & \frac{1}{G_j k_{\beta_j}^2}\left(v_j SH - k^2 \frac{SH'}{v_j'}\right) & 0 \\ 0 & 0 & -\frac{SH'}{G_j v_j'} \end{bmatrix} \tag{A-3b}$$

$$\boldsymbol{a}_{21} = \begin{bmatrix} G_j\left(\frac{-4k^2}{k_{\beta_j}^2}v_j SH + \frac{(2k^2-k_{\beta_j}^2)^2}{k_{\beta_j}^2}\frac{SH'}{v_j'}\right) & \frac{-2kG_j}{k_{\beta_j}^2}(2k^2-k_{\beta_j}^2)(CH-CH') & 0 \\ \frac{2kG_j}{k_{\beta_j}^2}(2k^2-k_{\beta_j}^2)(CH-CH') & G_j\left(\frac{(2k^2-k_{\beta_j}^2)^2}{k_{\beta_j}^2}\frac{SH}{v_j} - \frac{4k^2}{k_{\beta_j}^2}v_j' SH'\right) & 0 \\ 0 & 0 & -G_j\, v_j'\, SH' \end{bmatrix} \quad \text{(A-3c)}$$

$$\boldsymbol{a}_{22} = \begin{bmatrix} \frac{2k^2}{k_{\beta_j}^2}(CH-CH') + CH' & \frac{k}{k_{\beta_j}^2}\left(2v_j SH - (2k^2-k_{\beta_j}^2)\frac{SH'}{v_j'}\right) & 0 \\ \frac{k}{k_{\beta_j}^2}\left(2v_j' SH' - (2k^2-k_{\beta_j}^2)\frac{SH}{v_j}\right) & CH - \frac{2k^2}{k_{\beta_j}^2}(CH-CH') & 0 \\ 0 & 0 & CH' \end{bmatrix} \quad \text{(A-3d)}$$

in which $SH = sinhv_j\, d_j$, $SH' = sinhv_j'\, d_j$, $CH = coshv_j\, d_j$, and $CH' = coshv_j'\, d_j$.

REFERENCES

1. Ahmad, S. and A1-Hussaini, T. M., "Simplified Design for Vibration Screening by Open and In-Filled Trenches," *Journal of Geotech Engineering*, ASCE, **117**, pp. 67–88 (1991).
2. Lu, Jian-Fei., Xu, Bin. and Wang, Jian-Hun, "Numerical Analysis of Isolation of the Vibration Due to Moving Loads Using Pile Rows," *Journal of Sound and Vibration*, **319**, pp. 940–962 (2009).
3. Takemiya, H., "Field Vibration Mitigation by Honeycomb WIB for Pile Foundations of a High- Speed Train Viaduct," *Soil Dynamics and Earthquake Engineering*, **24**, pp. 69–87 (2004).
4. Sheng, X., Jones, C. J. C. and Petyt, M., "Ground Vibration Generated by a Load Moving Along a Railway Track," *Journal of Sound and Vibration*, **228**, pp. 129–156 (1999).
5. Krylov, V. V., "Vibrational Impact of High-Speed Trains. I. Effect of Track Dynamics," *Journal of the Acoustical Society of America*, **100**, pp. 3121–3134 (1996).
6. Kaynic, A. M., Madshus, C. and Zackrisson, P., "Ground Vibration from High-Speed Train: Prediction and Countermeasure," *Journal of Geotechnical and Geoenvironmental Engineering*, **126**, pp. 0531–0573 (2000).
7. Karlstrom, A., "An Analytical Model for Ground Vibrations from Accelerating Trains," *Journal of Sound and Vibration*, **293**, pp. 587–598 (2006).
8. Apsel, R. J. and Luco, J. E., "On the Green's Functions for a Layered Half-Space, Part II," *Bulletin of Seismological Society of America*, **73**, pp. 931–951 (1983).
9. Yeh, C.-S., Teng, T.-J., Liao, W.-I. and Chai, J.-F., "The Transition Matrix for the Scattering of Elastic Waves in a Half-Space," *Journal of the Chinese Institute of Engineers*, **30**, pp. 983–996 (2007).
10. Vostroukhov, A. V., Verichev, S. N., Kok, A. W. M. and Esveld, C., "Steady-State Response of a Stratified Half-Space Subjected to a Horizontal Arbitrary Buried Uniform Load Appied at a Circular Area," *Soil Dynamics and Earthquake Engineering*, **24**, pp. 449–459 (2004).
11. Liou, G.-S., "Vibrations Induced by Harmonic Loadings Applied at Circular Rigid Plate on Half-Space Medium," *Journal of Sound and Vibration*, **323**, pp. 257–269 (2009).
12. Liou, G.-S., "Further Investigation of Vibrations Induced by Harmonic Loadings Applied at Circular Rigid Plate on Half-Space Medium," *Journal of Chinese Institute of Engineers*, **34**, pp. 995–996 (2011).
13. Woods, R. D. and Larry, P. J., "Energy-Attenuation Relationships from Construction Vibrations," *Proceedings of Vibration Problems in Geotechnical Engineering Convention*, Detroit, Michigan, pp. 229–246 (1985).
14. Liou, G.-S. and Chung, I-L., "Impedance Matrices for Circular Foundation Embedded in Layered Medium," *Soil Dynamics Earthquake Engineering*, **29**, pp. 677–692 (2009).

(Manuscript received March 2, 2012,
accepted for publication July 13, 2012.)